RSC Advances

PAPER

Published on 19 November 2026
Licensed under CC-BY-NC 4.0

Check for updates

Cite this: DOI: 10.1039/d6ra08513j

Zinc oxide-containing material prepared in the presence of *Agrimonia eupatoria* extract: antimicrobial activity, effects on cell viability, and DNA damage responses

Katarina G. Marković,[a] Mirjana Ž. Grujović,[a] Đorđe Minić,*[b] Nevena Djukić,[b] Nadežda Radmilović,[c] Maja Popović,[c] Sanja Lj. Matić,[a] Milica Paunović,[b] Ana D. Obradović[b] and Ana Kesić[a]

A zinc oxide (ZnO)-containing material was prepared by alkaline precipitation of zinc acetate in the presence of an aqueous *Agrimonia eupatoria* extract, followed by thermal treatment at 200 °C. The material was characterized using UV-vis spectroscopy, Fourier-transform infrared spectroscopy (FTIR), transmission electron microscopy (TEM) with selected-area electron diffraction (SAED), and X-ray photoelectron spectroscopy (XPS). SAED revealed crystalline ZnO in the examined regions, while XPS indicated the presence of Zn(II) and organic and oxygen-containing surface species. The material exhibited strain-dependent antimicrobial activity, with minimum inhibitory concentrations (MICs) ranging from ≤78 to 10.000 μg mL^{-1}. MTT assays revealed concentration- and time-dependent changes in cell viability in cancer and non-malignant cell lines; however, the absence of cell-free interference controls and an independent viability assay limit the interpretation of these findings. Changes in assay signals associated with superoxide production, nitrite accumulation and total NF-κB p65 levels were also observed. In the *Drosophila melanogaster* comet assay, the two lowest tested concentrations (0.25 and 0.5 mg mL^{-1}) did not produce a detectable increase in comet scores, whereas higher concentrations were associated with increased scores. Co-exposure with ethyl methanesulphonate (EMS) resulted in lower comet scores than EMS treatment alone, particularly at lower concentrations, but these observations do not establish a specific DNA-protective mechanism. The absence of plant-free ZnO and extract-only controls, bulk X-ray diffraction (XRD), and measurements of Zn^{2+} release under biological exposure conditions limits the attribution of the observed effects to individual components. Overall, the findings describe the antimicrobial and cell-based responses associated with the tested ZnO-containing preparation and highlight the need for further controlled studies to clarify its composition and biological effects.

Received 7th September 2026
Accepted 9th November 2026

DOI: 10.1039/d6ra08513j

rsc.li/rsc-advances

1 Introduction

The rapid emergence of antimicrobial resistance, alongside the increasing global burden of cancer, has intensified the search for novel, effective, and biocompatible therapeutic agents. In this context, nanotechnology has emerged as a promising interdisciplinary field, offering innovative solutions through the development of nanoscale materials with enhanced physicochemical and biological properties.[1,2] Among these, zinc oxide nanoparticles (ZnO NPs) have attracted considerable attention due to their unique optical, catalytic, and biological characteristics.[3,4]

ZnO NPs exhibit a broad spectrum of biological activities, including antimicrobial, cytotoxic, and antioxidant effects, which are largely attributed to their ability to generate reactive oxygen species (ROS), disrupt cellular membranes, and interact with intracellular components.[1,2,5] Their antimicrobial activity has been demonstrated against a wide range of Gram-positive and Gram-negative bacteria, as well as fungi, making them potential candidates for combating resistant pathogens.[6] ZnO NPs have been reported to exert cytotoxic effects on cancer and non-cancerous cells, with the degree of selectivity depending on nanoparticle characteristics, concentration, exposure time, and cell type.[5,7]

[a]*University of Kragujevac, Institute for Information Technologies, Department of Natural Sciences, Liceja Kneževine Srbije 1A, 34000 Kragujevac, Serbia*

[b]*University of Kragujevac, Faculty of Science, Department of Biology and Ecology, Radoja Domanovica 12, 34000 Kragujevac, Serbia. E-mail: djordje.minic@pmf.kg.ac.rs*

[c]*University of Belgrade, Vinca Institute of Nuclear Sciences, National Institute of the Republic of Serbia, Department of Atomic Physics, Mike Petrovića Alasa 12-14, 11000 Belgrade, Serbia*

© 2026 The Author(s). Published by the Royal Society of Chemistry

Conventional methods for nanoparticle synthesis, including physical and chemical approaches, often involve toxic reagents, high energy consumption, and environmentally hazardous by-products.[8–10] These limitations have driven the development of green synthesis strategies, which utilize biological systems such as plant extracts, microorganisms, and biomolecules as sources of bioactive and surface-active compounds that can influence nanoparticle formation and surface properties.[10,11] Plant-mediated synthesis is particularly attractive because of its simplicity, scalability, and the presence of diverse phytochemicals that can interact with metal precursors and influence the physicochemical and surface properties of the resulting nanomaterials.[12,13] In contrast to the synthesis of elemental metal nanoparticles, where plant-derived compounds may participate directly in the reduction of metal ions, the formation of metal oxide nanoparticles may also involve hydrolysis, precipitation, and subsequent thermal conversion of the metal precursor. In such systems, plant phytochemicals may contribute to surface association, surface modification, and potentially particle growth characteristics rather than acting as the sole driving force for nanoparticle formation.

A. eupatoria L. (Rosaceae family), commonly known as agrimony, a medicinal plant widely used in traditional medicine, is rich in bioactive compounds such as flavonoids, tannins, and phenolic acids, which exhibit antimicrobial, antioxidant, and anti-inflammatory properties.[14] These phytochemicals may interact with metal-containing precursors or intermediate species and may contribute to surface modification of the resulting nanomaterials.[15]

Despite the growing interest in ZnO-containing materials, studies addressing their combined antimicrobial activity, effects on cell viability, and DNA-damaging and DNA-damage-modulating properties remain relevant. Assessment of DNA damage is important for evaluating potential biological effects, while studies of DNA-damage modulation can provide information on changes in chemically induced DNA damage under specific experimental conditions. In the present study, a ZnO-containing material was prepared in the presence of an aqueous extract of *Agrimonia eupatoria* and characterized using physicochemical methods. Its antimicrobial activity against selected microorganisms, effects on the viability of cancer and non-malignant cell lines, and effects on DNA damage and EMS-induced comet scores were investigated. The study describes the biological responses observed under the tested conditions without attributing them to a specific component of the preparation.

2 Experimental

2.1 Chemicals

Zinc acetate was purchased from Sigma-Aldrich (St. Louis, MO, USA), while sodium hydroxide was obtained from Hemos d.o.o. (Belgrade, Serbia). Phosphate-buffered saline (PBS) without calcium and magnesium, normal melting-point agarose (NMA), low-melting-point agarose (LMA), ethidium bromide, and collagenase were purchased from Alfa Trade Enterprise d.o.o. (Belgrade, Serbia). Ethyl methanesulphonate (EMS) was obtained from Sigma-Aldrich (St. Louis, MO, USA). Mueller–Hinton broth and Sabouraud dextrose broth were purchased from Torlak (Belgrade, Serbia). Doxycycline was obtained from Sigma Chemicals Co. (St. Louis, MO, USA), whereas ketoconazole was supplied by Hemofarm A.D. (Vršac, Serbia). Resazurin was purchased from Alfa Aesar GmbH & Co. KG (Karlsruhe, Germany).

2.2 Preparation of the ZnO-containing material

A ZnO-containing material was prepared in the presence of an aqueous extract of *Agrimonia eupatoria* L. The aerial parts of the plant were collected during the flowering stage on Mount Bukulja, Serbia, identified at the Faculty of Science, University of Kragujevac, and air-dried in the dark at ambient temperature.[14] The dried plant material was ground and macerated in distilled water three times at room temperature, using fresh solvent for each 24 h extraction period. The extracts were filtered, and the combined filtrates were evaporated to dryness using a rotary evaporator at 40 °C. The dried extract was stored at 4 °C until use.[14,15]

For the preparation of the ZnO-containing material, 30 mL of 0.1 M zinc acetate solution was mixed with 20 mL of an aqueous *A. eupatoria* extract. The pH was adjusted to approximately 13 by adding 0.1 M NaOH, with the pH monitored using indicator strips. The reaction mixture, with a total volume of approximately 50 mL, was stirred at 6000 rpm at 25 °C for 2 h. At the end of the reaction, the suspension appeared white to pale yellow. The resulting solid was separated by centrifugation, and the pellet was collected. The pellet was washed three times with distilled water and twice with 70% ethanol. Finally, the washed pellet was dried in a drying oven at 200 °C for 2 h. Under the strong alkaline reaction conditions, hydrolysis and precipitation of zinc-containing species may occur independently of the plant-derived compounds, followed by thermal conversion to ZnO. The aqueous *A. eupatoria* extract was therefore considered a potential source of compounds that may associate with or modify the surface of the resulting material. Since a plant-free control prepared under identical conditions was not included, the specific contribution of the extract to material formation and physicochemical properties could not be established. Zinc remains in the +2-oxidation state during ZnO formation; therefore, the extract is not considered a reducing agent in this process.

For brevity, the resulting material is referred to as ZnO-containing material throughout this study. This designation describes the ZnO-containing preparation obtained in the presence of the plant extract and does not imply that its properties or biological effects arise exclusively from ZnO nanoparticles. The material was characterized using UV-vis spectroscopy, transmission electron microscopy (TEM), Fourier-transform infrared (FTIR) spectroscopy, and X-ray photoelectron spectroscopy (XPS), as described below.

2.3 Physicochemical characterization of the ZnO-containing material

The physicochemical properties of the ZnO-containing material were investigated using UV-vis spectroscopy, Fourier-transform

© 2026 The Author(s). Published by the Royal Society of Chemistry

infrared (FTIR) spectroscopy, transmission electron microscopy (TEM), and X-ray photoelectron spectroscopy (XPS).

FTIR spectra were recorded using a PerkinElmer Spectrum Two spectrometer equipped with a universal attenuated total reflectance (UATR) accessory. The samples were analyzed directly, without further preparation. Spectra were recorded over the range of 4000–400 cm^{-1}, using 16 scans per sample at a resolution of 4 cm^{-1}. The spectra were processed using Spectrum™ 10 software for baseline correction and normalization.

Transmission electron microscopy was performed using an FEI Talos F200X microscope equipped with an X-FEG source and operated at an accelerating voltage of up to 200 keV. Conventional TEM, high-resolution TEM (HRTEM), scanning transmission electron microscopy (STEM), and high-angle annular dark-field (HAADF) imaging were performed. Energy-dispersive X-ray spectroscopy (EDS) was used for spatially resolved elemental mapping. For sample preparation, the solid powder was dispersed in ethanol, and a drop of the resulting suspension was deposited onto a carbon-coated copper grid and allowed to dry in air. Interplanar spacings corresponding to characteristic crystalline planes in individual particles were measured using ImageJ software.[16]

The surface chemical composition and bonding states of the elements in the ZnO-containing material were investigated using X-ray photoelectron spectroscopy (XPS). Before analysis, the sample was dried in an oven at 40 °C for 24 h and mounted on copper tape. Measurements were performed using a SPECS system equipped with a monochromatic Al Kα X-ray source operating at 12.5 kV and 250 W. The base pressure in the analysis chamber was below 5×10^{-7} Pa. Spectra were acquired in fixed analyzer transmission (FAT) mode. Survey spectra were recorded over the binding-energy range from −5 to 1000 eV, with a step size of 0.5 eV, a dwell time of 0.2 s, and a pass energy of 40 eV. High-resolution spectra were acquired using a pass energy of 20 eV, a step size of 0.1 eV, and a dwell time of 0.2 s. Data acquisition was controlled using SpecsLab software, and the spectra were processed using CasaXPS.

2.4 Antimicrobial activity of the ZnO-containing material

2.4.1 Tested microorganisms. The antimicrobial activity of the tested ZnO-containing material was evaluated against bacterial and fungal strains, including reference strains obtained from the American Type Culture Collection (ATCC) and non-ATCC isolates. The bacterial panel comprised *Staphylococcus aureus* ATCC 25923, *Bacillus subtilis* ATCC 6633, *Enterococcus faecalis* ATCC 29212, *Escherichia coli* ATCC 25922, *Pseudomonas aeruginosa* ATCC 27853, and *Proteus mirabilis* ATCC 12453, together with non-ATCC strains of *Staphylococcus aureus*, *Bacillus subtilis*, *Bacillus cereus*, *Bifidobacterium animalis* subsp. *lactis*, *Enterococcus faecalis*, *Escherichia coli*, *Salmonella enterica*, *Salmonella typhimurium*, *Proteus mirabilis*, and *Klebsiella pneumoniae*.

The fungal panel included the reference strains *Candida albicans* ATCC 10231, *Aspergillus flavus* ATCC 9170, and *Aspergillus niger* ATCC 16404, as well as non-ATCC strains of *Penicillium italicum* and *Penicillium chrysogenum*. The clinical isolates were provided by the Institute of Public Health, Kragujevac, Serbia. The remaining microorganisms, including the fungal strains and ATCC reference strains, were obtained from the collection maintained by the Microbiology Laboratory, Faculty of Science, University of Kragujevac, Serbia.

2.4.2 Microdilution method. The antimicrobial activity of the ZnO-containing material was evaluated using a resazurin-based microdilution assay to determine the minimum inhibitory concentration (MIC) and minimum microbicidal concentration (MMC). Twofold serial dilutions of the tested material were prepared in sterile 96-well microplates containing 100 μL of Mueller–Hinton broth for bacteria or Sabouraud dextrose broth for fungi. The final concentration range was 78–10.000 μg mL^{-1}. When inhibition was observed at the lowest concentration tested, the MIC was reported as ≤78 μg mL^{-1}.

Microbial suspensions were adjusted to a turbidity equivalent to the 0.5 McFarland standard and subsequently diluted to obtain final inoculum densities of 5×10^5 CFU mL^{-1} for bacteria and 5×10^3 CFU mL^{-1} for fungi. The prepared microbial suspensions were used as inoculum in the microdilution assay.

Microbial growth was assessed using resazurin, a redox indicator that changes color from blue to pink when reduced by metabolically active cells, as described previously.[17] The plates were incubated at 37 °C for 24 h for bacteria, and at 28 °C for 48 h for yeasts and 72 h for filamentous fungi. The MIC was defined as the lowest concentration that prevented the resazurin colour change. For filamentous fungi, inhibition of visible mycelial growth was also assessed.

The MMC was determined by subculturing 10 μL from wells showing no visible growth onto nutrient agar plates. The lowest concentration at which no colony formation was observed after incubation was recorded as the MMC. Doxycycline, dissolved in Mueller–Hinton broth, was used as the antibacterial reference compound, while ketoconazole, prepared in Sabouraud dextrose broth, was used as the antifungal reference compound. Growth and sterility controls were included, and all experiments were performed in three independent experiments.

2.5 Effects of the ZnO-containing material on cell lines

2.5.1 Cell cultivation and treatment procedure. The human lung fibroblast cell line MRC-5, the mouse macrophage cell line RAW 264.7, the human breast cancer cell line MDA-MB-231, and the human colon cancer cell line HCT-116 were obtained from the American Type Culture Collection (ATCC, Manassas, VA, USA). MRC-5 cells were used as a non-malignant comparator. RAW 264.7 cells were analyzed separately and were not considered a non-malignant reference.

All cell lines were cultured in Dulbecco's modified Eagle's medium (DMEM) supplemented with 10% foetal bovine serum (FBS) and an antibiotic solution containing penicillin (100 IU mL^{-1}) and streptomycin (100 μg mL^{-1}). The cells were maintained at 37 °C in a humidified atmosphere containing 5% CO_2.

Cells were cultured in flasks until they reached approximately 80% confluence and were then seeded into 96-well plates

© 2026 The Author(s). Published by the Royal Society of Chemistry

for cell viability assays or 6-well plates for ELISA analyses, at densities of 1×10^4 and 1×10^6 cells per well, respectively. The plates were incubated at 37 °C in a humidified atmosphere containing 5% CO_2 to allow cell attachment. After attachment, the cells were exposed to the tested ZnO-containing material at concentrations of 1, 10, 25, 50, 100, and 150 μg mL^{-1} for 24 h or 72 h.

For RAW 264.7 cells, an LPS-stimulated inflammatory model was established by adding lipopolysaccharide (LPS) from *Escherichia coli* at a concentration of 1 μg mL^{-1}, 1 h before treatment with the tested material. Cell viability was assessed in all four cell lines. Superoxide-associated and nitrite levels were measured in the cell models specified in the respective assay procedures. NF-κB p65 levels were determined in RAW 264.7 cells after short-term exposure to the lower concentrations of 1 and 10 μg mL^{-1}. Untreated cells served as controls, and experiments were performed in triplicate.

The stock suspensions of the tested material were prepared in DMEM containing 1% DMSO to a final concentration of 1 mg mL^{-1} and dispersed using a vortex before further dilution in culture medium. Stock suspensions were then diluted in DMEM to reach the required working concentrations. In the working solution with the minimal concentration, the final DMSO content was kept at or below approximately 0.001% (v/v). Particle size and colloidal stability in the culture medium were not assessed.

2.5.2 Assessment of cell viability by the MTT assay. Cell viability was assessed using the MTT assay, which is based on the reduction of thiazolyl blue tetrazolium bromide to formazan by metabolically active cells.[18] Following treatment with the tested material, the culture medium was replaced with 100 μL of fresh culture medium containing 25 μL of MTT solution (5 mg mL^{-1}). The cells were incubated for 4 h at 37 °C in a humidified atmosphere containing 5% CO_2. After incubation, the MTT-containing solution was removed, and the resulting formazan crystals were dissolved in 150 μL of dimethyl sulphoxide (DMSO) per well. Absorbance was measured at 550 nm using an ELISA plate reader.

Cell viability was expressed as a percentage of the absorbance measured in untreated control cells, which was defined as 100%. Apparent half-maximal inhibitory concentrations (IC_{50}) were estimated from the concentration–response data using CalcuSyn software. Cell-free controls containing the tested material and MTT reagent in the absence of cells were not included; therefore, potential interference of the tested material with the assay signal could not be excluded.

2.5.3 NBT reduction assay. Superoxide-associated signals were assessed using the nitro blue tetrazolium (NBT) assay.[19] The assay is based on the reduction of NBT to insoluble nitroblue formazan. Following the experimental treatment, 20 μL of NBT solution (5 mg mL^{-1}) was added to each well, and the plates were incubated for 1 h at 37 °C in a humidified atmosphere containing 5% CO_2. The resulting formazan was solubilized using 20 μL of dimethyl sulphoxide (DMSO), and absorbance was measured at 550 nm.

The measured absorbance was used as an indicator of NBT reduction under the experimental conditions. Cell-free controls containing the tested material were not included, and the signal was not normalized to the number of viable cells. Therefore, the results were interpreted as changes in the NBT assay signal rather than as a direct quantitative measurement of intracellular superoxide concentration.

2.5.4 Assessment of nitrite levels using the Griess assay. Nitrite levels (NO_2^-), used as an indirect indicator of nitric oxide (NO) production, were assessed using the Griess reaction.[20] The assay is based on the formation of a diazonium intermediate from nitrite under acidic conditions, followed by reaction with *N*-(1-naphthyl)ethylenediamine to form a colored azo dye. The Griess reagent was freshly prepared by mixing equal volumes of 0.1% *N*-(1-naphthyl)ethylenediamine dihydrochloride and 1% sulfanilamide in 5% phosphoric acid. After a 10 min incubation, absorbance was measured at 550 nm. Nitrite levels were expressed as μmol NO_2^- per mL. Cell-free controls were not included, and the measured signals were not normalized to viable cell numbers. Consequently, potential interference of the tested material with the assay signal could not be excluded, and the results were interpreted as changes in the Griess assay signal rather than as direct evidence of altered NO production.

2.5.5 Measurement of total NF-κB p65 concentration. NF-κB p65 levels were determined using an ELISA kit (Elabscience, Houston, TX, USA), following the manufacturer's instructions. Following treatment, the cells were detached using trypsin, centrifuged, washed with phosphate-buffered saline (PBS), and subjected to sonication. The resulting supernatants were collected for analysis. Briefly, 100 μL of each supernatant was added to microtiter wells pre-coated with an antibody specific for NF-κB p65 and incubated for 90 min at room temperature. Without an intervening washing step, the biotinylated detection antibody solution was added, and the plate was incubated for a further 1 h. After the prescribed washing steps, the horseradish peroxidase (HRP) conjugate was added and incubated for 30 min. The substrate solution was then added, and the plate was incubated for 15 min in the dark at room temperature. The reaction was stopped by adding 50 μL of stop solution to each well. Absorbance was measured at 450 nm, and NF-κB p65 concentrations were calculated using a standard curve.

The assay measured total NF-κB p65 in the cell lysates and did not assess its phosphorylation, nuclear translocation, or transcriptional activity. The results were not normalized to viable cell number; therefore, changes in the measured concentration should be interpreted cautiously, particularly under conditions associated with reduced cell viability.

2.6 DNA damage and changes in EMS-associated comet scores

The DNA-damaging and DNA-damage-modulating effects of the tested ZnO-containing material were investigated in *Drosophila melanogaster* using the alkaline comet assay. Wild-type Canton-S flies and larvae were obtained from the Bloomington Stock Centre, Indiana, USA, and reared on standard nutritive medium containing agar, sugar, and yeast. The flies were maintained in glass bottles under controlled conditions at 25 °C, 60% relative humidity, and a 12 h light/12 h dark cycle.

© 2026 The Author(s). Published by the Royal Society of Chemistry

Third-instar *D. melanogaster* larvae (74 ± 2 h old) were transferred to standard Drosophila corn medium without or with ethyl methanesulphonate (EMS; 1 mM in PBS), which served as the negative and positive control treatments, respectively.[21]

Zinc acetate dihydrate ($Zn(CH_3COO)_2 \cdot 2H_2O$) was included as a soluble zinc comparator at three nominal concentrations corresponding to the lowest, an intermediate, and the highest concentrations tested for the ZnO-containing material. This comparator provided a qualitative reference for exposure to soluble zinc. However, zinc-ion release from the tested material was not quantified under the exposure conditions, and the zinc acetate treatments were matched by nominal mass concentration rather than by measured Zn^{2+} exposure. Assuming pure ZnO, zinc acetate dihydrate at 0.25, 1, and 4 mg mL^{-1} corresponds to 0.074, 0.298, and 1.19 mg Zn per mL, respectively, whereas ZnO at nominal concentrations of 0.25–4 mg mL^{-1} corresponds to a maximum elemental zinc content of approximately 0.201–3.21 mg Zn per mL. Thus, at the same nominal mass concentration, the zinc acetate comparator provided approximately 2.7-fold less elemental zinc than pure ZnO. These treatments therefore do not permit a direct assessment of the relative contribution of soluble zinc ions to the observed effects.

For DNA-damage assessment, groups of ten larvae were exposed to 24 h in individual vials containing standard Drosophila food supplemented with the tested material at concentrations of 0.25, 0.5, 1, 2, and 4 mg mL^{-1}. To investigate changes in EMS-induced DNA damage, groups of ten larvae were co-exposed for 24 h to the same concentrations of the tested material and 1 mM EMS. Following exposure, the larvae from each vial (98 ± 2 h old) were collected, and cell suspensions were prepared from the anterior midguts of all ten larvae pooled together.[22,23] The alkaline comet assay was performed according to ref. 24 with minor modifications.[22]

The tested material was dispersed in phosphate-buffered saline (PBS) and then incorporated into the food. Its dispersion state in the food medium was not characterized.

Fluorescence images were acquired using a Nikon Ti-Eclipse fluorescence microscope equipped with a charge-coupled device (CCD) camera and a 40× objective lens. One comet assay slide was prepared from each cell suspension. Three independent experiments were performed for each treatment, with one exposure vial and one corresponding slide per experiment. Thus, the exposure vial and its pooled larval sample represented the experimental unit, whereas individual cells scored on the slide were not considered independent experimental replicates.

2.7 Statistical analysis

Statistical analyses were performed using SPSS software, version 20.0 (SPSS Inc., Chicago, IL, USA). Data are presented as mean ± standard error of the mean (SEM) from three independent experiments, unless otherwise stated. For the comet assay, data are presented as mean ± standard deviation (SD) from three independent experiments. Differences among treatment groups were evaluated using one-way analysis of variance (ANOVA), followed by Bonferroni's or Dunnett's *post hoc* test, as appropriate. Statistical significance was set at $p < 0.05$.

Apparent IC_{50} values were calculated using CalcuSyn software (BIOSOFT, Cambridge, UK). Selectivity indices (SI), where reported, were calculated as the ratio of the apparent IC_{50} value for MRC-5 cells to that for the corresponding cancer cell line. These indices were treated as exploratory numerical comparisons, as no formal statistical comparison between dose–response curves were performed. The IC_{50} estimates were not independently validated using an orthogonal cell viability assay, and potential interference with the MTT assay could not be excluded.

For the comet assay, the independent exposure vial containing the pooled larval sample was considered the experimental unit ($n = 3$ per treatment). Individual cells or images were not considered independent experimental replicates.

3 Results

3.1 Preparation and preliminary characterization of the ZnO-containing material

The preparation of the ZnO-containing material in the presence of the aqueous *Agrimonia eupatoria* extract was monitored by UV-vis spectrophotometry. The spectrum of the plant extract showed characteristic absorption in the ultraviolet region, consistent with the presence of UV-absorbing phytochemical constituents. For the preparation, 30 mL of 0.1 M zinc acetate solution was mixed with the plant extract 20 mL, and the pH was adjusted to 13 using 0.1 M NaOH. The reaction was conducted at 25 °C for 2 h, during which the suspension developed a white-to-pale-yellow appearance.

No pronounced time-dependent changes in the UV-vis spectra were detected following the addition of the zinc precursor. After thermal treatment at 200 °C, a distinct absorption maximum appeared at approximately 370 nm (Fig. 1). The corresponding wavelength-based estimate of the optical band gap was approximately 3.35 eV, calculated using (E_g\approx 1240/\lambda), where (\lambda) is expressed in nanometers. This value is consistent with previously reported optical band-gap values for ZnO-based materials.[25–27]

The appearance of the absorption maximum after thermal treatment, rather than during the initial reaction in the liquid phase, is consistent with the formation or development of ZnO-related optical properties during the subsequent processing step. However, the absence of a distinct absorption feature before thermal treatment does not exclude the formation of zinc-containing precursor or intermediate species during the alkaline reaction.

The strongly alkaline conditions used in the preparation are relevant to the interpretation of the synthesis process. At pH 13, zinc-containing hydroxide species may form through hydrolysis and precipitation, followed by conversion during thermal treatment. Accordingly, the formation of the ZnO-containing material cannot be attributed exclusively to the plant extract.

The extract may nevertheless contribute to the surface characteristics of the final material. The FTIR and XPS results

© 2026 The Author(s). Published by the Royal Society of Chemistry

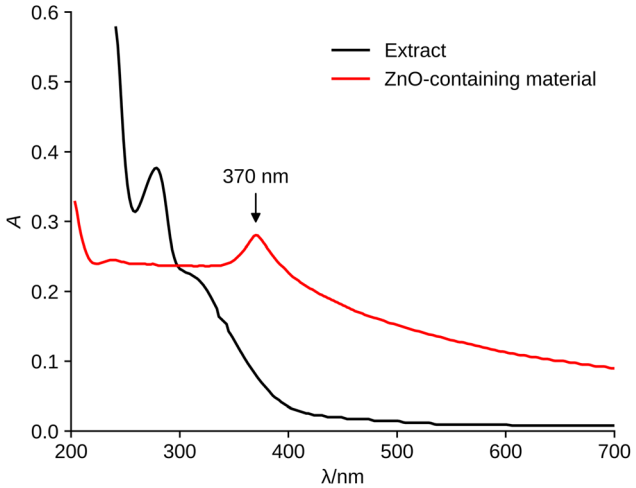


Fig. 1 UV-Vis absorption spectra of the aqueous *A. eupatoria* extract (black line) and the ZnO-containing material after thermal treatment at 200 °C (red line).

presented below are consistent with the presence of organic and oxygen-containing species associated with the material's surface. However, because a plant-free control prepared under otherwise identical conditions was not available, the specific contribution of *A. eupatoria* constituents to particle formation, morphology, crystallinity, surface chemistry, or biological activity could not be established. The observed results are therefore attributed to the tested ZnO-containing preparation.

3.2 Physicochemical characterization of the ZnO-containing material

3.2.1 FTIR analysis. Fourier-transform infrared (FTIR) spectroscopy was used to investigate the functional groups present in the *A. eupatoria* extract and the ZnO-containing material (Fig. 2). The spectra showed overlapping absorption features, consistent with the presence of organic functional groups in the extract and in the final material.

The spectrum of the plant extract exhibited a broad absorption band in the 3200–3500 cm^{-1} region, which was assigned to O–H stretching vibrations associated with hydroxyl-containing compounds. A band in the 1570–1650 cm^{-1} region may be associated with C=C and/or C=O vibrations, while bands in the 1400–1000 cm^{-1} region may correspond to C–O, C–N and C–O–C vibrations of organic constituents.

The spectrum of the ZnO-containing material showed a broad band around 3300 cm^{-1}, which may be associated with surface hydroxyl groups, adsorbed water and/or residual organic compounds. Additional bands were observed in the 1630–1550 cm^{-1} region and at 1403, 1288, 1154 and 1074 cm^{-1}. These features are consistent with the presence of oxygen-containing organic functional groups. A strong band at approximately 455 cm^{-1}, accompanied by weaker bands in the 600–650 cm^{-1} region, was assigned to Zn–O-related lattice vibrations.

Overall, the FTIR spectra support the presence of functional groups consistent with organic and oxygen-containing species in the tested material. However, FTIR analysis alone cannot establish the identity or origin of individual surface species, nor can it determine whether the extract contributed directly to the formation of the ZnO phase or became associated with the material during subsequent processing.

3.2.2 TEM and crystalline features revealed by SAED. TEM, high-resolution TEM (HRTEM), selected-area electron diffraction (SAED) and high-angle annular dark-field scanning transmission electron microscopy (HAADF-STEM) were used to examine the morphology and crystalline features of the tested material (Fig. 3 and 4).

TEM images revealed irregularly shaped particles, including structures composed of elongated, rod-like features extending from a common center and producing a petal-like appearance (Fig. 3a). Measurement of 50 individual particles showed sizes ranging from approximately 40 to 220 nm, with most measured

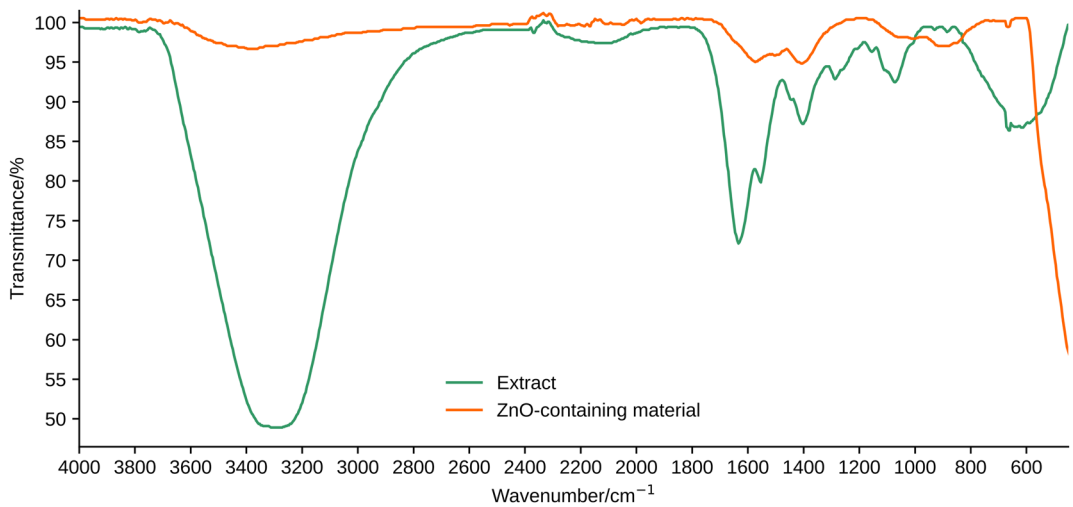


Fig. 2 FTIR spectra of the aqueous *A. eupatoria* extract and the ZnO-containing material prepared in its presence.

© 2026 The Author(s). Published by the Royal Society of Chemistry

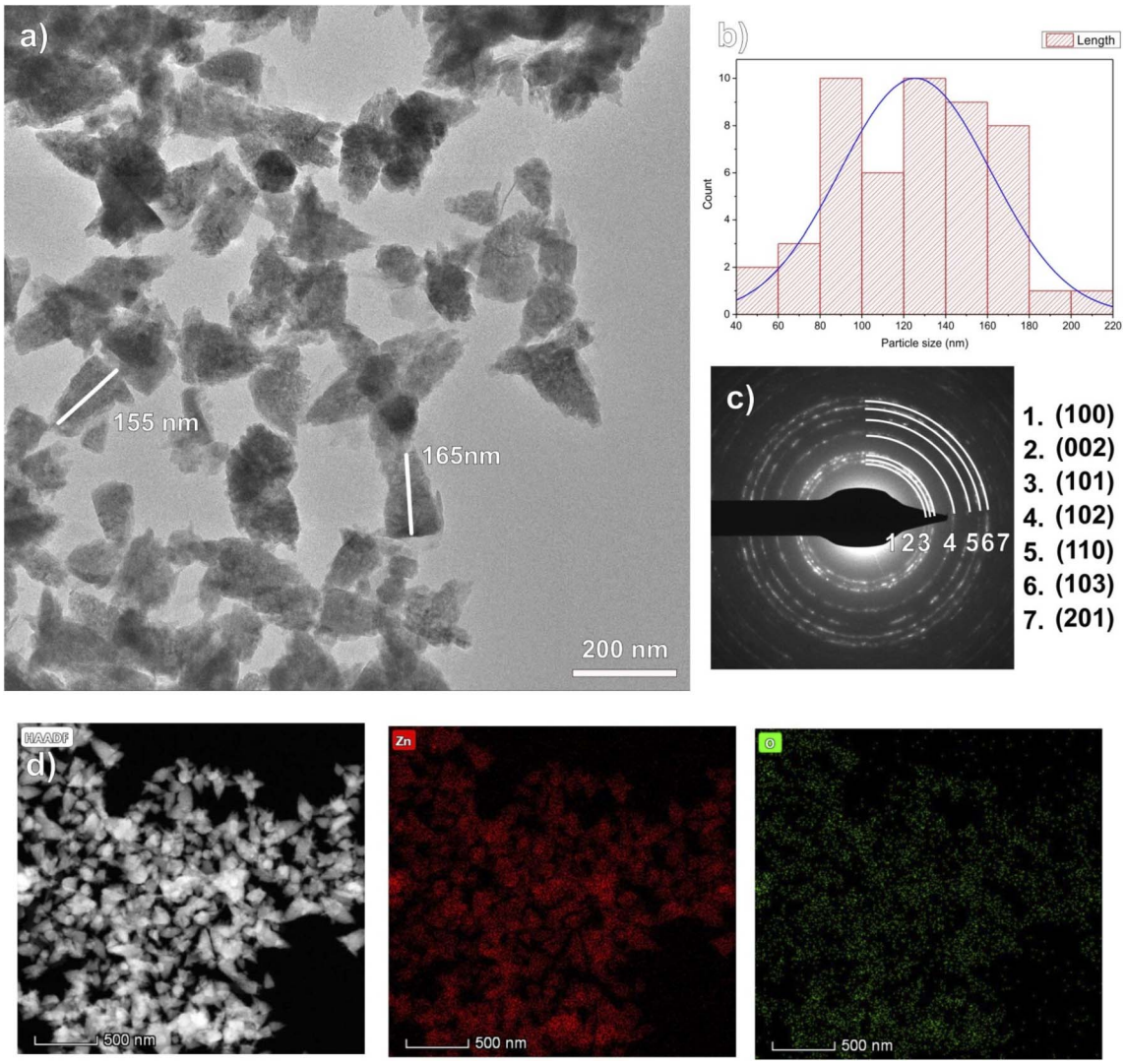


Fig. 3 Morphology and chemical composition of the ZnO-containing material: (a) TEM micrograph showing representative morphology; (b) particle size distribution histogram; (c) SAED pattern with diffraction rings corresponding to the (100), (002), (101), (102), (110), (103), and (201) crystallographic planes; (d) HAADF micrograph with elemental maps of zinc and oxygen.

particles falling within the 80–180 nm range (Fig. 3b). Representative particles measured approximately 155 and 165 nm along their longest dimensions. These measurements describe the dimensions of particles observed on dried TEM grids and do not establish their hydrodynamic size or degree of aggregation in biological media.

The SAED pattern showed diffraction rings consistent with crystalline hexagonal ZnO, with reflections indexed to the (100), (002), (101), (102), (110), (103) and (201) planes (Fig. 3c), in agreement with reference data for ZnO (JCPDS Card No. 36-1451). Similar patterns were observed in the examined regions. These findings provide evidence for crystalline ZnO in the analyzed areas; however, the bulk phase composition and purity of the entire powder cannot be established from SAED alone.

HAADF-STEM imaging and elemental mapping showed Zn and O distributed across the analyzed particle regions (Fig. 3d). HRTEM images revealed ordered lattice fringes consistent with the crystalline structure observed by SAED (Fig. 4a). The mean interplanar spacing was calculated as 2.56 Å by measuring 50 consecutive lattice fringes in the inverse fast Fourier transform (IFFT) image (Fig. 4c). This value is consistent with the expected spacing of the (002) planes of hexagonal ZnO. The images also showed elongated crystalline features; however, quantitative aspect-ratio analysis was not performed.

Taken together, TEM and SAED provide evidence for particles with irregular and elongated morphologies and crystalline ZnO features in the examined regions. Because powder X-ray diffraction (XRD) was not performed, the bulk phase composition and phase purity of the material remain unconfirmed, and the presence of residual zinc-containing phases cannot be excluded.

3.2.3 XPS analysis. X-ray photoelectron spectroscopy (XPS) was used to investigate the surface elemental composition and chemical states of the tested material (Fig. 5). The survey

© 2026 The Author(s). Published by the Royal Society of Chemistry

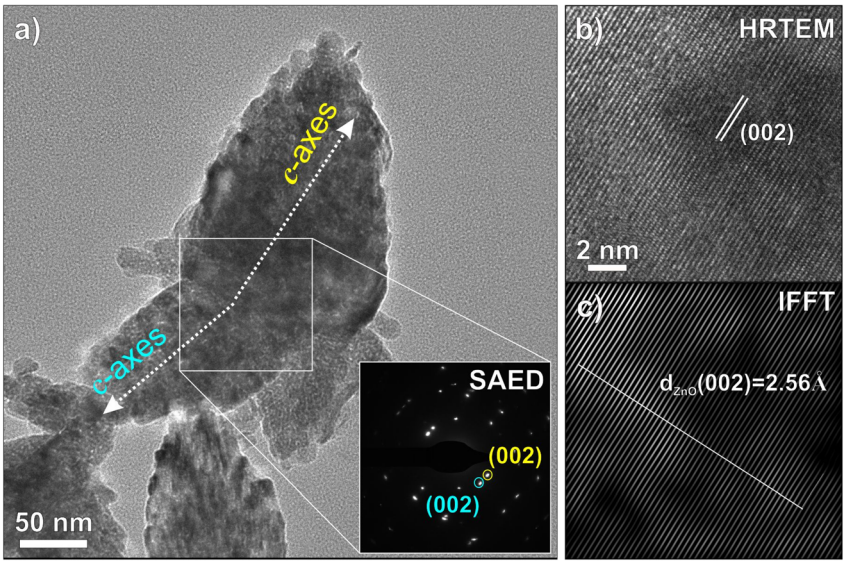


Fig. 4 Structural analysis of the ZnO-containing material: (a) HRTEM image with an inset showing the diffraction pattern and particle elongation along the *c*-axis; (b) HRTEM micrograph showing well-resolved (002) lattice planes; (c) inverse fast Fourier transform (IFFT) image used to measure an interplanar spacing of 2.56 Å.

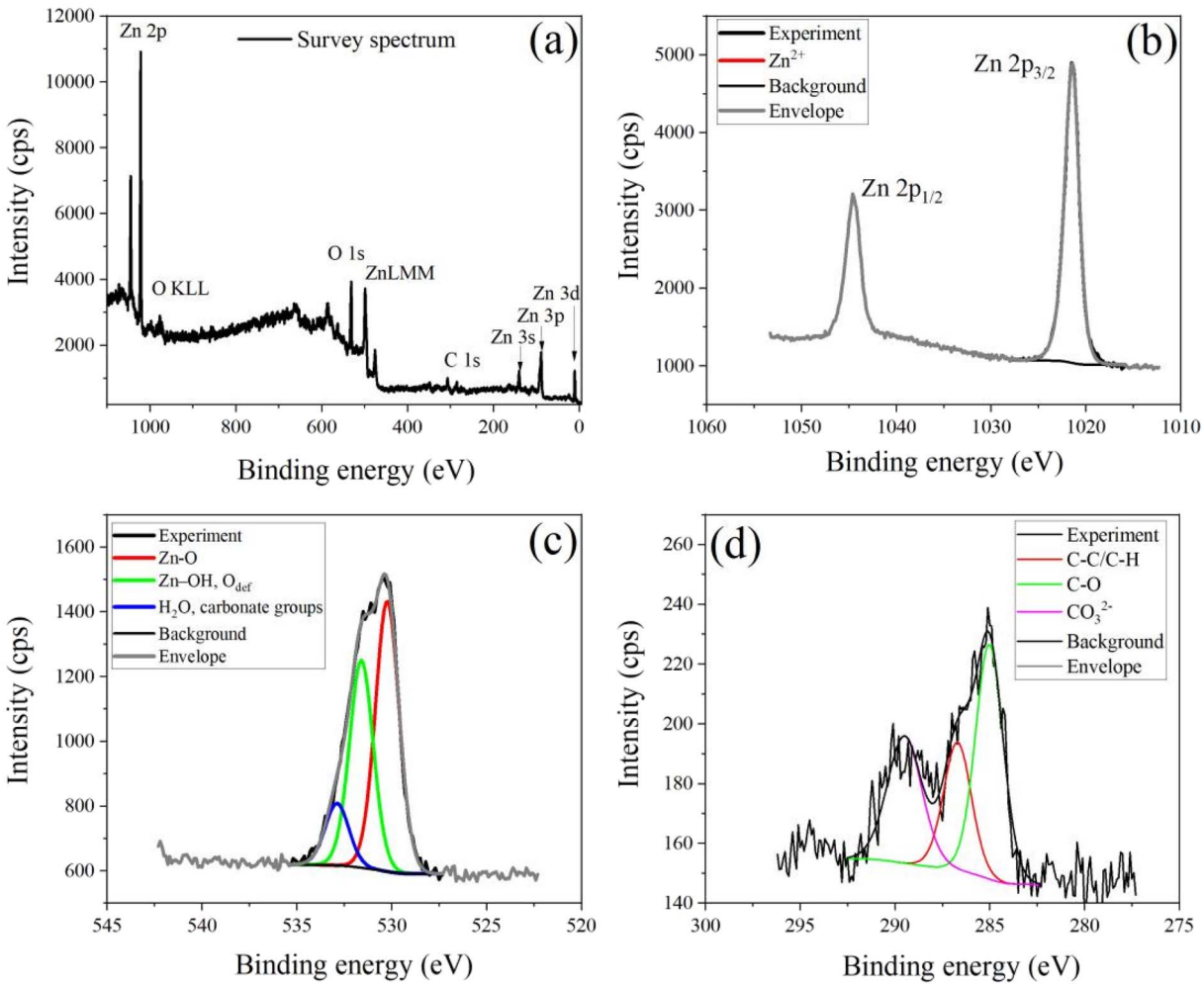


Fig. 5 X-ray photoelectron spectroscopy (XPS) analysis of the ZnO-containing material: (a) survey spectrum showing the presence of Zn, O, and C; (b) high-resolution Zn 2p spectrum showing the Zn $2p_{3/2}$ and Zn $2p_{1/2}$ core levels characteristic of Zn(II); (c) O 1s spectrum deconvoluted into components assigned to lattice oxygen, surface hydroxyl groups/defect-related oxygen species, and adsorbed species; (d) C 1s spectrum indicating the presence of adventitious carbon, C–O bonds, and carbonate species.

© 2026 The Author(s). Published by the Royal Society of Chemistry

spectrum showed signals corresponding primarily to zinc, oxygen and carbon (Fig. 5a). The main Zn 2p peaks occurred at approximately 1022 and 1045 eV, while the O 1s and C 1s signals were observed around 531 and 285 eV, respectively. Additional features were assigned to oxygen and zinc Auger transitions.

Quantitative analysis of the survey spectrum indicated an apparent surface composition of approximately 30 at% Zn, 50 at% O and 20 at% C. After excluding carbon from the calculation, the recalculated Zn ratio was approximately 38 : 62 (O/Zn $\approx$ 1.65). This oxygen-rich surface composition, relative to the stoichiometric Zn ratio of bulk ZnO, may reflect contributions from surface hydroxyl groups and other oxygen-containing species. The result should be interpreted as a surface-sensitive measurement rather than a determination of the bulk elemental composition.

The high-resolution Zn 2p spectrum showed peaks at 1021.5 and 1044.5 eV (Fig. 5b), with a spin–orbit separation of approximately 23.02 eV. These features are consistent with zinc predominantly in the +2 oxidation state. No distinct metallic zinc contribution was detected in the analyzed spectrum.

The O 1s spectrum was fitted with three components centered at 530.2, 531.6 and 532.9 eV (Fig. 5c). These components were assigned, respectively, to lattice oxygen in Zn–O bonds, surface hydroxyl and other non-lattice oxygen species, and adsorbed oxygen-containing species, potentially including water and carbonate species. Their relative contributions were approximately 50%, 38% and 12% of the fitted O 1s signal, respectively.

The C 1s spectrum contained components at approximately 285.0, 286.7 and 289.5 eV (Fig. 5d). These were assigned to C–C/C–H, C–O-containing groups and carbonate-related species, respectively. The presence of C–O-containing groups is consistent with organic species at the material surface, but XPS alone cannot establish whether these species originated from the plant extract, adventitious contamination or other sources.

Overall, the XPS results are consistent with a ZnO-containing material whose surface contains zinc predominantly in the +2-oxidation state, lattice oxygen, hydroxyl and other oxygen-containing species, and carbon-containing components. In combination with the FTIR and TEM/SAED results, these findings support the presence of crystalline ZnO features and a chemically heterogeneous surface in the analyzed material. However, neither the specific origin of the surface organic species nor the bulk phase purity of the powder can be established from these measurements alone.

3.3 Antimicrobial activity of the ZnO-containing material

The antimicrobial activity of the tested ZnO-containing material was evaluated against a panel of Gram-positive and Gram-negative bacteria and fungal strains. The minimum inhibitory concentration (MIC) and minimum microbicidal concentration (MMC) were determined using a microdilution assay and compared with doxycycline and ketoconazole as reference antibacterial and antifungal compounds, respectively (Table 1).

The antibacterial activity varied considerably among the tested strains. The lowest MIC values were recorded for *Staphylococcus aureus* and *S. aureus* ATCC 25923, for which inhibition was observed at the lowest concentration tested (78 $\mu g\ mL^{-1}$). The corresponding MMC values were 312.5 and 120 $\mu g\ mL^{-1}$, respectively. Because inhibition was already observed at the lowest tested concentration, the exact MIC values for these strains could not be established without extending the concentration range below 78 $\mu g\ mL^{-1}$.

Among the other bacterial strains, the lowest MIC values were observed for *Salmonella typhimurium* (312.5 $\mu g\ mL^{-1}$) and *Klebsiella pneumoniae* (625 $\mu g\ mL^{-1}$). The MIC was 625 $\mu g\ mL^{-1}$ for *Bacillus subtilis* ATCC 6633 and 1250 $\mu g\ mL^{-1}$ for the non-ATCC *B. subtilis* strain. For *E. coli* and *E. coli* ATCC 25922, the MIC was 1250 $\mu g\ mL^{-1}$, with an MMC of 2500 $\mu g\ mL^{-1}$ for both strains. The non-ATCC *Proteus mirabilis* strain showed an MIC of 1250 $\mu g\ mL^{-1}$ and an MMC of 2500 $\mu g\ mL^{-1}$, whereas *P. mirabilis* ATCC 12453 showed an MIC of 5000 $\mu g\ mL^{-1}$ and an MMC of 10.000 $\mu g\ mL^{-1}$. The MIC and MMC values for *Salmonella enterica* were 2500 and 5000 $\mu g\ mL^{-1}$, respectively.

Lower susceptibility was observed for several other bacterial strains. The MIC and MMC were both 10.000 $\mu g\ mL^{-1}$ for *Bacillus cereus*, *Bifidobacterium animalis* subsp. *lactis*, *Enterococcus faecalis* and *E. faecalis* ATCC 29212. The same values were recorded for *Pseudomonas aeruginosa* ATCC 27853. These findings demonstrate that the antimicrobial response was strain-dependent, with substantial differences between the MIC values recorded across the bacterial panel.

The antifungal activity also differed among the tested strains. For *P. chrysogenum* and *A. niger* ATCC 16404, inhibition was observed at the lowest concentration tested (78 $\mu g\ mL^{-1}$), and the exact MIC could therefore not be determined. The MMC was $\leq$78 $\mu g\ mL^{-1}$ for *P. chrysogenum*, whereas the MMC for *A. niger* ATCC 16404 was 5000 $\mu g\ mL^{-1}$. The MIC and MMC values for *Candida albicans* ATCC 10231 were 10.000 and greater than 10.000 $\mu g\ mL^{-1}$, respectively. *Aspergillus flavus* ATCC 9170 showed an MIC of 5000 $\mu g\ mL^{-1}$ and an MMC of 10.000 $\mu g\ mL^{-1}$. The MIC for *P. italicum* was 156.2 $\mu g\ mL^{-1}$, while MMC reported for this strain was 10.000 $\mu g\ mL^{-1}$.

The results obtained with the reference compounds are presented in Table 1. Doxycycline was used as the antibacterial reference and ketoconazole as the antifungal reference. Their MIC and MMC values provide a comparison with the activity of the tested preparation under the experimental conditions. However, the reference compounds and the tested material differ in chemical composition and mode of action; therefore, the numerical differences in MIC values should be interpreted as an assay-based comparison rather than evidence of equivalent antimicrobial potency.

The observed antimicrobial activity may be associated with physicochemical interactions between the tested material and microbial cells. Possible mechanisms proposed for ZnO-containing materials include the release of Zn^{2+} ions, interactions with microbial cell surfaces and the generation of reactive oxygen species. These processes may affect membrane integrity, cellular components and metabolic functions.[28–35] However, Zn^{2+} release, nanoparticle dissolution and reactive oxygen species generation were not directly investigated in the present study. Furthermore, plant-free ZnO and aqueous-extract-only

© 2026 The Author(s). Published by the Royal Society of Chemistry

Table 1 Antimicrobial activity of the tested ZnO-containing preparation and reference antimicrobial compounds[a]

Species	Preparation MIC (μg mL^{-1})	Preparation MMC (μg mL^{-1})	Doxycycline MIC (μg mL^{-1})	Doxycycline MMC (μg mL^{-1})	Ketoconazole MIC (μg mL^{-1})	Ketoconazole MMC (μg mL^{-1})
Staphylococcus aureus	≤78	312.5	0.45	7.81	—	—
Staphylococcus aureus ATCC 25923	≤78	117	0.224	3.75	—	—
Bacillus subtilis	1250	10 000	0.112	1.953	—	—
Bacillus subtilis ATCC 6633	625	10 000	1.953	31.25	—	—
Bacillus cereus	10 000	10 000	0.977	7.81	—	—
Bifidobacterium animalis subsp. *lactis*	10 000	10 000	4	16	—	—
Enterococcus faecalis	10 000	10 000	2	8	—	—
Enterococcus faecalis ATCC 29212	10 000	10 000	4	12	—	—
Escherichia coli	1250	2500	15.63	62.5	—	—
Escherichia coli ATCC 25922	1250	2500	15.63	31.25	—	—
Pseudomonas aeruginosa ATCC 27853	10 000	10 000	62.5	125	—	—
Salmonella enterica	2500	5000	15.63	31.25	—	—
Salmonella typhimurium	312.5	2500	2	4	—	—
Proteus mirabilis ATCC 12453	5000	10 000	7.81	15.63	—	—
Proteus mirabilis	1250	2500	15.63	62.5	—	—
Klebsiella pneumoniae	625	1250	8	32	—	—
Candida albicans ATCC 10231	10 000	>10 000	—	—	1.96	1.96
Penicillium italicum	156.2	10 000	—	—	<0.49	<0.49
Penicillium chrysogenum	≤78	≤78	—	—	31.25	62.5
Aspergillus flavus ATCC 9170	5000	10 000	—	—	<0.49	1.96
Aspergillus niger ATCC 16404	≤78	5000	—	—	31.25	62.5

[a] Abbreviations: MIC, minimum inhibitory concentration; MMC, minimum microbicidal concentration. Values are expressed in μg mL^{-1}. "≤78" indicates that the endpoint was reached at the lowest concentration tested (78 μg mL^{-1}); the actual endpoint was not determined because lower concentrations were not tested. "—" indicates that the reference antimicrobial was not applicable to the respective microorganism. Doxycycline was used as the reference antibacterial compound, whereas ketoconazole was used as the reference antifungal compound. The results refer to the tested ZnO-containing preparation obtained in the presence of *Agrimonia eupatoria* aqueous extract. In the absence of plant-free ZnO and extract-only controls, the contribution of individual components to the observed antimicrobial activity cannot be determined.

controls were not included. Consequently, the relative contributions of the ZnO-containing material and extract-derived constituents to the observed antimicrobial effects cannot be determined.

The aqueous *A. eupatoria* extract has previously been investigated against some of the microorganisms included in the present study.[14] In that separate investigation, higher MIC values for the extract than for the tested ZnO-containing preparation were reported for *S. aureus* ATCC 25923, *K. pneumoniae*, *S. Typhimurium*, *P. chrysogenum* and *A. niger* ATCC 16404. Similar MIC values were reported for *P. aeruginosa* ATCC 27853, whereas lower MIC values were reported for *B. cereus*, *B. animalis* subsp. *lactis* and *E. faecalis* ATCC 29212. These findings provide context for the present results but do not constitute a direct comparison, because the extract and the tested preparation were not evaluated concurrently under identical experimental conditions. Accordingly, the contribution of the extract to the antimicrobial activity of the preparation cannot be established from these data.

Overall, the tested ZnO-containing material showed variable inhibitory and microbicidal activity across the bacterial and fungal strains examined. The differences in MIC and MMC values indicate that susceptibility depended on the microorganism tested. Further experiments incorporating plant-free ZnO controls, extract-only controls and independent confirmation of the antimicrobial endpoints are required to determine the contribution of individual components and to establish the reproducibility of the observed effects.

3.4 Effects on cell viability and cellular assay signals

3.4.1 MTT-based cell viability and apparent IC_{50} values. The effects of the tested ZnO-containing preparation on cell viability were evaluated in MRC-5 fibroblasts, RAW 264.7 macrophages, MDA-MB-231 breast cancer cells, and HCT-116 colorectal cancer cells (Fig. 6 and Table 2). The response varied according to cell type and exposure duration.

After 24 h of exposure, the apparent MTT-based IC_{50} values were 44.73 ± 2.12 μg mL^{-1} for MRC-5 cells, 26.65 ± 0.53 μg mL^{-1} for RAW 264.7 cells, 81.31 ± 2.51 μg mL^{-1} for MDA-MB-231 cells, and 71.82 ± 2.18 μg mL^{-1} for HCT-116 cells. After 72 h, the corresponding values were 52.13 ± 1.93, 40.15 ± 1.25, 58.67 ± 1.02, and 14.04 ± 0.54 μg mL^{-1}, respectively.

The numerical comparison with MRC-5 fibroblasts yielded selectivity indices (SI) of 0.55 and 0.62 for MDA-MB-231 and HCT-116 cells, respectively, after 24 h. Following 72 h of exposure, the corresponding SI values were 0.89 for MDA-MB-231 cells and 3.71 for HCT-116 cells. These ratios are exploratory

© 2026 The Author(s). Published by the Royal Society of Chemistry

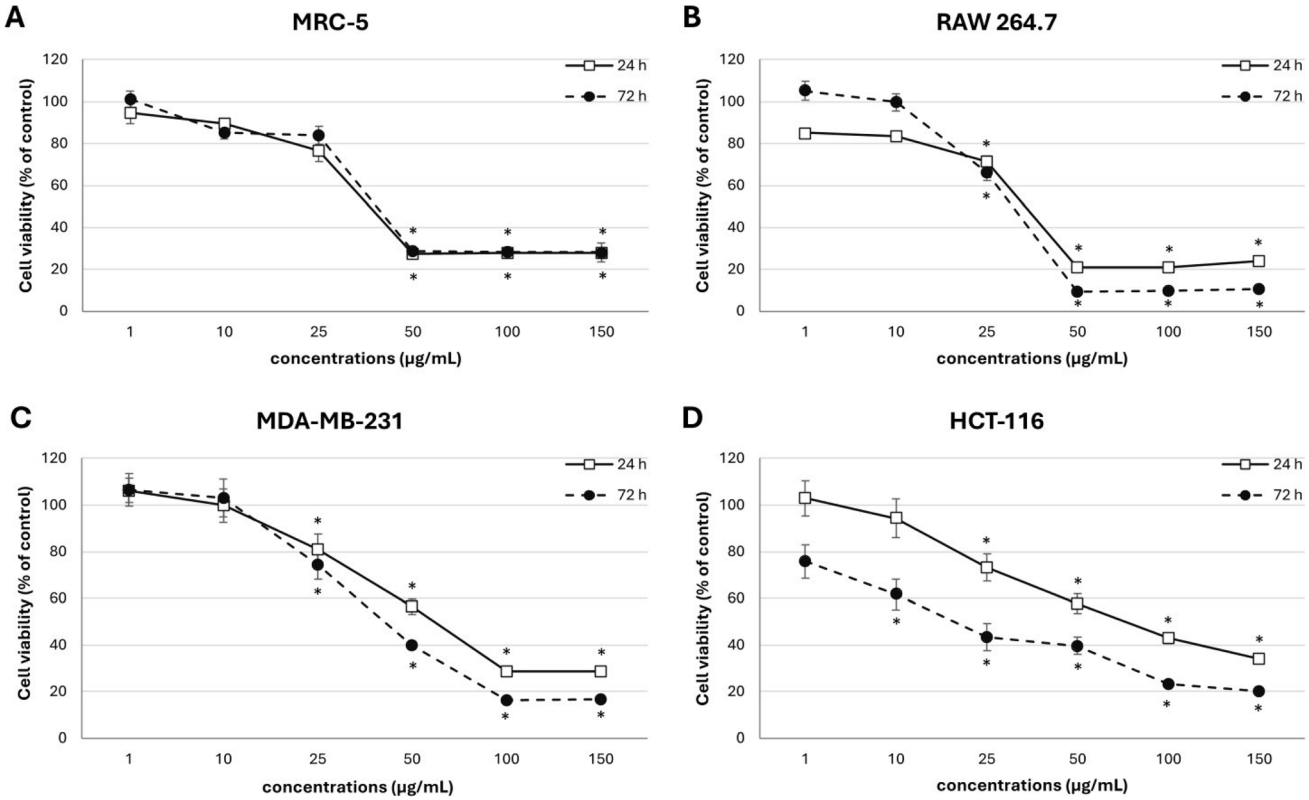


Fig. 6 Effects of the tested ZnO-containing preparation on the viability of MRC-5 (A), RAW 264.7 (B), MDA-MB-231 (C), and HCT-116 (D) cells after 24 and 72 h of exposure. The results are presented as the mean ± standard error of three independent experiments. *$p < 0.05$ compared with untreated control cells.

Table 2 Apparent MTT-based IC_{50} values of the tested ZnO-containing preparation in MRC-5, RAW 264.7, MDA-MB-231 and HCT-116 cells[a]

Cell line/parameter	IC_{50} (μg mL^{-1}), 24 h	IC_{50} (μg mL^{-1}), 72 h
MRC-5	44.73 ± 2.12	52.13 ± 1.93
RAW 264.7	26.65 ± 0.53	40.15 ± 1.25
MDA-MB-231	81.31 ± 2.51	58.67 ± 1.02
HCT-116	71.82 ± 2.18	14.04 ± 0.54
SI (MRC-5/MDA-MB-231)	0.55	0.89
SI (MRC-5/HCT-116)	0.62	3.71

[a] IC_{50} values are presented as mean ± standard error of three independent experiments. The reported IC_{50} values are apparent MTT-based estimates and have not been independently validated using an orthogonal cell viability assay. Selectivity indices (SI), were calculated as the ratio of the apparent IC_{50} value for MRC-5 cells to that for the corresponding cancer cell line. These ratios are exploratory numerical comparisons; no formal statistical comparison between dose–response curves was performed. RAW 264.7 cells were analysed separately as a transformed murine macrophage cell line and were not used as a non-malignant reference. Potential interference with the MTT assay could not be completely excluded.

comparisons and do not, by themselves, demonstrate statistically significant preferential cytotoxicity. In particular, the lower apparent IC_{50} observed for HCT-116 cells after 72 h requires further confirmation. RAW 264.7 cells were considered separately as a macrophage model and were not used as a non-malignant comparator.

The results indicate cell-type- and exposure-time-dependent changes in the MTT assay signal. However, cell-free controls containing the tested preparation and MTT reagent were not included. Regarding the timing and method of adding the MTT reagent to the wells containing cells, potential interference between the tested preparation and the MTT reagent cannot be completely excluded, but it was limited. Nevertheless, the calculated IC_{50} values should be regarded as apparent MTT-based estimates rather than independently validated measures of cytotoxicity. The data do not establish selective anticancer activity.

3.4.2 Changes in NBT and Griess assay signals and total NF-κB p65 levels. The effects of the tested ZnO-containing preparation on redox-associated responses were investigated in RAW 264.7, MDA-MB-231 and HCT-116 cells following short- and long-term exposure to concentrations ranging from 1 to 50 μg mL^{-1} (Fig. 7). The responses varied depending on the cell line, concentration and exposure duration.

In RAW 264.7 cells (Fig. 7A), short-term exposure to 1 and 10 μg mL^{-1} was associated with a slight reduction in the NBT assay signal, whereas long-term exposure to 25 and 50 μg mL^{-1} resulted in a significant increase compared with the control. In MDA-MB-231 cells (Fig. 7C), significant reductions in the NBT assay signal were observed after 24 h at 10 and 25 μg mL^{-1} and after 72 h at 1 and 10 μg mL^{-1}. In contrast, HCT-116 cells (Fig. 7E) showed no significant changes under the tested conditions.

© 2026 The Author(s). Published by the Royal Society of Chemistry

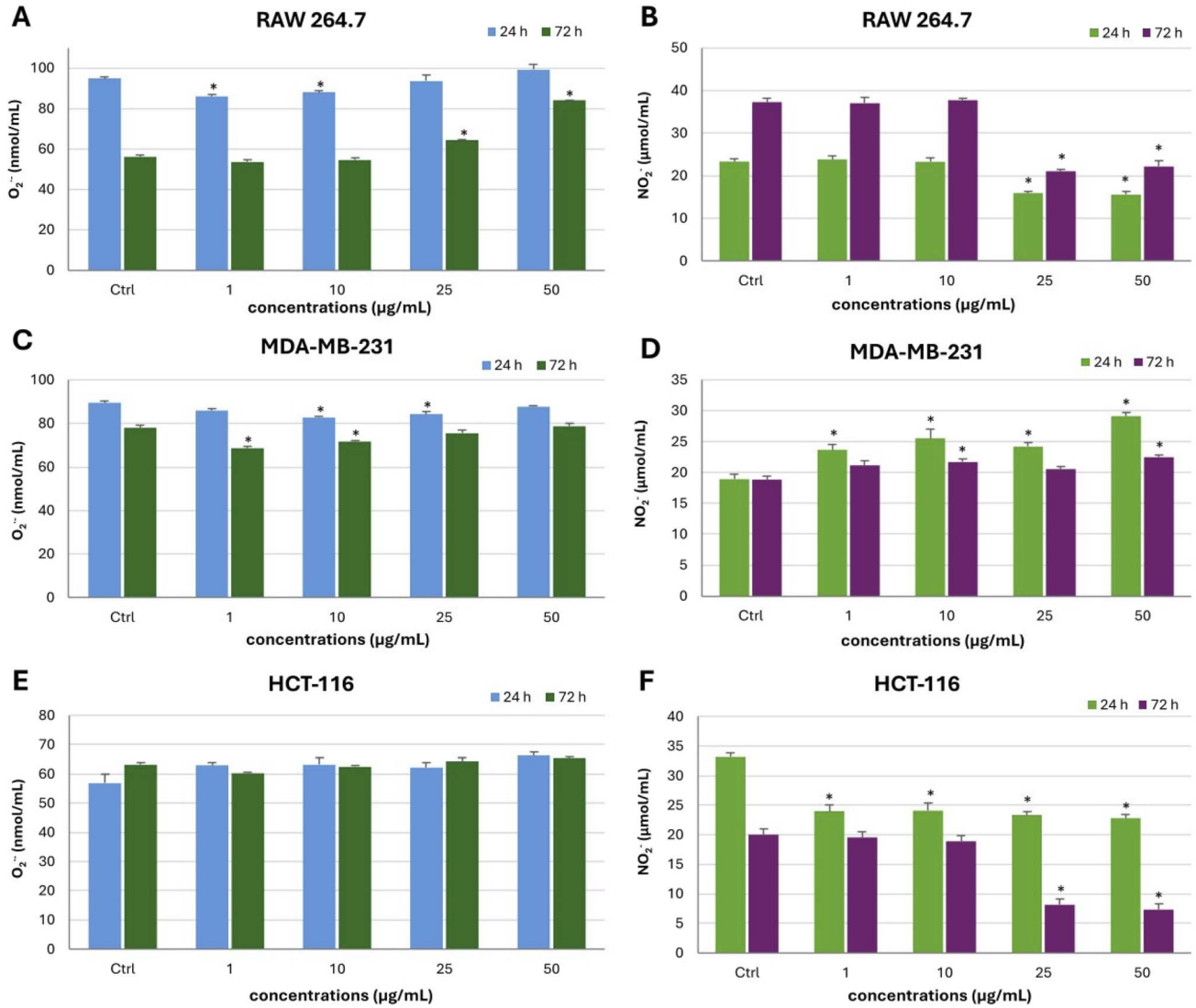


Fig. 7 Effects of the tested ZnO-containing preparation on NBT reduction and nitrite-associated assay signals in RAW 264.7 (A and B), MDA-MB-231 (C and D), and HCT-116 (E and F) cells after 24 and 72 h of exposure. The results are presented as the mean ± standard error of three independent experiments. *$p < 0.05$ compared with untreated control cells.

The Griess assay also revealed cell-type-dependent responses (Fig. 7B, D and F). In RAW 264.7 cells, exposure to 25 and 50 μg mL^{-1} was associated with reduced nitrite-associated signals at both time points. Conversely, MDA-MB-231 cells showed increased Griess assay signals under almost all tested conditions. HCT-116 cells exhibited a concentration-dependent decrease in the Griess assay signal compared with the control.

The effects of the tested preparation on inflammatory-associated responses were further investigated in LPS-stimulated RAW 264.7 macrophages (Fig. 8). The preparation was administered 1 h after LPS stimulation at concentrations of 1, 10, 25 and 50 μg mL^{-1} for the NBT and Griess assays and at concentrations of 1 and 10 μg mL^{-1} for the NF-κB p65 ELISA. Cell viability was also evaluated over the concentration range of 1–150 μg mL^{-1}.

The MTT assay results for LPS-stimulated RAW 264.7 cells (Fig. 8A) showed a significant concentration-dependent reduction in the assay signal compared with both untreated cells and cells treated with LPS alone. LPS treatment significantly reduced cell viability after 24 h, whereas no significant effect was observed after 72 h. At 1 and 10 μg mL^{-1}, the tested preparation did not significantly affect the MTT assay signal after prolonged exposure. Following 24 h of exposure, however, a significant reduction was observed in the group treated with 10 μg mL^{-1} compared with the control groups. A similar response was observed in RAW 264.7 cells without LPS stimulation (Fig. 6B).

Changes in the NBT assay signal in LPS-stimulated RAW 264.7 cells are shown in Fig. 8C. After 24 h, all tested concentrations except 50 μg mL^{-1} were associated with a decrease in the signal compared with the control group. After 72 h, lower concentrations did not produce statistically significant changes, whereas higher concentrations were associated with increased signals compared with the control and LPS-treated groups.

© 2026 The Author(s). Published by the Royal Society of Chemistry

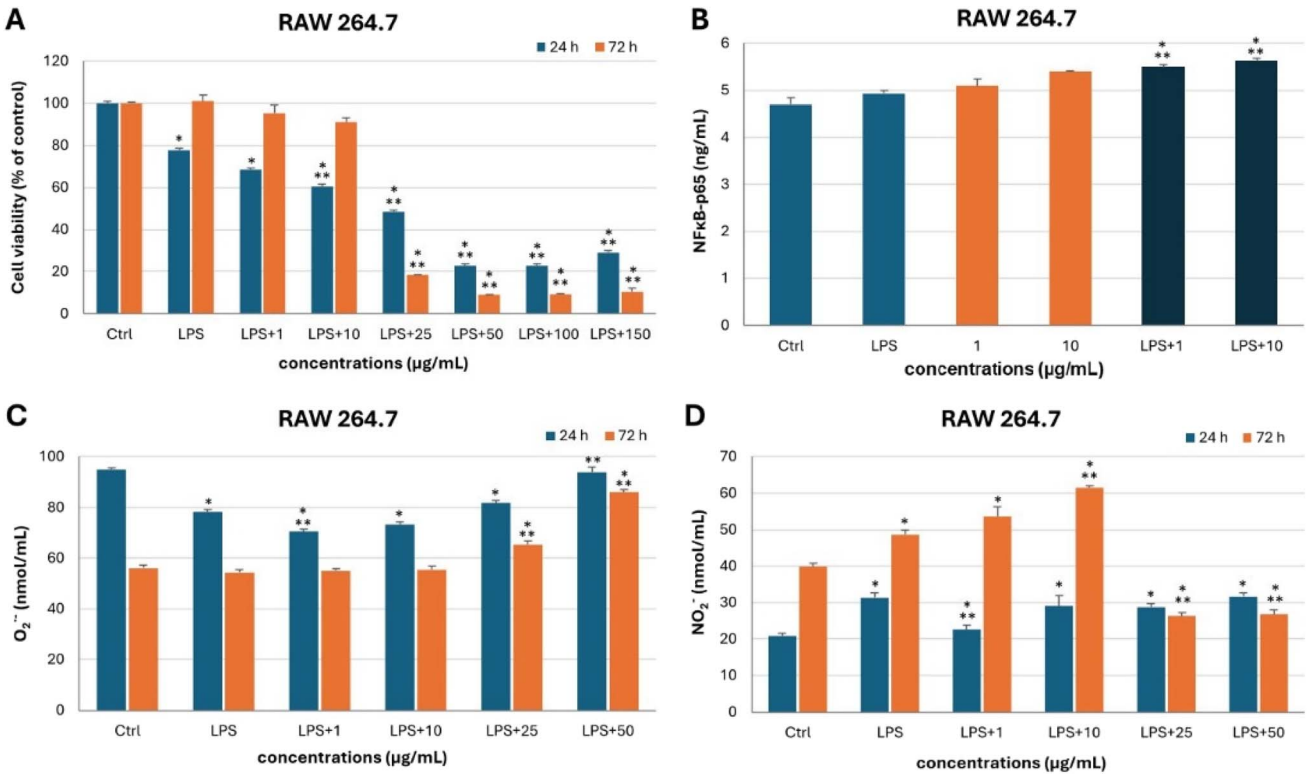


Fig. 8 Effects of the tested ZnO-containing preparation on LPS-stimulated RAW 264.7 cells: (A) cell viability; (B) total NF-κB p65 levels; (C) NBT reduction assay signal; and (D) nitrite-associated assay signal. The results are presented as the mean ± standard error of three independent experiments. *p < 0.05 compared with untreated control cells; **p < 0.05 compared with LPS-stimulated cells.

The Griess assay results for LPS-stimulated RAW 264.7 cells are presented in Fig. 8D. LPS treatment increased the nitrite-associated signal compared with the untreated control. After 24 h of exposure to the tested preparation, all concentrations were associated with lower signals than those observed in the LPS-treated control and untreated cells. After 72 h, higher concentrations also reduced the signal, whereas the lower concentrations of 1 and 10 μg mL^{-1} were associated with increased signals compared with the control groups. These findings indicate that the response depended on both concentration and exposure duration.

NF-κB p65 levels in RAW 264.7 cells after 24 h of exposure are presented in Fig. 8B. Treatment with LPS alone or with the tested preparation in the absence of LPS resulted in a slight, non-significant increase in the measured p65 levels. In LPS-stimulated cells, treatment with the preparation at 1 and 10 μg mL^{-1} significantly increased NF-κB p65 levels compared with the control groups. These findings do not support the interpretation that the tested preparation directly suppressed inflammatory signaling under the conditions examined.

Overall, the results demonstrate changes in NBT and Griess assay signals and in total NF-κB p65 levels, with responses varying according to cell type, concentration and exposure duration. However, the NBT assay measures the reduction of a tetrazolium reagent, while the Griess assay measures nitrite as an indirect indicator of nitric oxide production. Cell-free controls were not included for either assay, or the results were not normalized to viable cell number. Consequently, direct effects of the tested preparation on assay reagents and the influence of changes in cell viability cannot be excluded. In addition, the ELISA measured total NF-κB p65 concentration and did not assess its phosphorylation, nuclear translocation or transcriptional activity. The observed changes therefore cannot establish activation or inhibition of the NF-κB pathway or confirm an anti-inflammatory effect.

The interpretation of these findings is further limited by the absence of direct measurements of intracellular reactive oxygen species, zinc-ion release, mitochondrial dysfunction, apoptosis and caspase activation. Moreover, pro-inflammatory cytokines, including TNF-α, IL-6 and IL-1β, were not measured. Although redox-related processes have been proposed as contributors to the biological effects of ZnO-containing materials in previous studies,[35–45] the present results do not establish a causal relationship between the measured assay responses and cytotoxicity. Further studies incorporating appropriate cell-free interference controls, viability-normalized measurements, direct intracellular redox assays and complementary inflammatory markers are needed to clarify these responses.

3.5 DNA damage and changes in EMS-associated comet scores

The DNA-damaging and DNA-damage-modulating effects of the tested ZnO-containing material were investigated in *Drosophila melanogaster* using the alkaline comet assay. The results are presented in Table 3.

© 2026 The Author(s). Published by the Royal Society of Chemistry

Table 3 DNA damage and changes in EMS-associated comet scores following exposure to the ZnO-containing preparation obtained in the presence of an aqueous *A. eupatoria* extract[a]

Treatments [b]	Comet type[c]					TCS[d]	% *R*[e]
	CT_0	CT_1	CT_2	CT_3	CT_4		
NC	72.9 ± 0.16	27.1 ± 0.71	—	—	—	27.1 ± 0.32†	—
PC	24.9 ± 0.21	45.3 ± 0.16	24.1 ± 0.51	4.5 ± 0.32	1.2 ± 0.12	111.8 ± 1.17$^{*\ddagger\$£}$	—
$ZnA_{0.25}$	73.1 ± 0.24	26.9 ± 0.52	—	—	—	26.9 ± 0.32†	—
ZnA_1	72.6 ± 0.82	27.4 ± 0.17	—	—	—	27.4 ± 0.52†	—
ZnA_4	72.39 ± 0.17	27.61 ± 0.51	—	—	—	27.61 ± 0.71†	—
$ZnNP_{0.25}$	72.7 ± 0.32	27.3 ± 0.92	—	—	—	27.3 ± 0.25†	—
$ZnNP_{0.5}$	72.4 ± 0.21	27.6 ± 0.33	—	—	—	27.6 ± 0.34†	—
$ZnNP_1$	70.7 ± 0.52	27.2 ± 0.45	2.1 ± 0.34	—	—	31.4 ± 0.68$^{*\dagger\ddagger\$£}$	—
$ZnNP_2$	60.7 ± 0.64	35.8 ± 0.67	3.5 ± 0.32	—	—	42.8 ± 0.23$^{*\dagger\ddagger\$£}$	—
$ZnNP_4$	54.16 ± 0.84	41.64 ± 0.60	4.2 ± 0.13	—	—	50.04 ± 0.11$^{*\dagger\ddagger\$£}$	—
$ZnNP_{0.25}$ + EMS	57.2 ± 0.18	37.2 ± 0.17	5.6 ± 0.82	—	—	48.4 ± 0.34$^{*\dagger\ddagger\$£}$	74.8
$ZnNP_{0.5}$ + EMS	48.62 ± 0.13	45.56 ± 0.15	5.82 ± 0.19	—	—	57.2 ± 0.17$^{*\dagger\ddagger\$£}$	64.5
$ZnNP_1$ + EMS	51.25 ± 0.27	34.9 ± 0.24	12.65 ± 0.28	1.2 ± 0.22	—	63.8 ± 0.31$^{*\dagger\ddagger\$£}$	56.7
$ZnNP_2$ + EMS	47.9 ± 0.62	29.4 ± 0.62	18.4 ± 0.34	4.3 ± 0.52	—	79.1 ± 0.11$^{*\dagger\ddagger\$£}$	38.6
$ZnNP_4$ + EMS	49.49 ± 0.47	23.71 ± 0.38	20.1 ± 0.80	6.7 ± 0.33	—	84.01 ± 0.33$^{*\dagger\ddagger\$£}$	32.8

[a] "— indicates that no cells were recorded in the corresponding comet-damage category or percentage reduction could not be calculated for that treatment. Statistical significance: $^{*}p < 0.05$ *vs.* NC; $^{\dagger}p < 0.05$ *vs.* PC; $^{\ddagger}p < 0.05$ *vs.* ZnA0.25; $^{\$}p < 0.05$ *vs.* ZnA1; $^{£}p < 0.05$ *vs.* ZnA4". [b] The values are mean ± S.D. from three independent experiments. [c] CT, Comet Type defined as CT_0, CT_1, CT_2, CT_3, and CT_4 (no or meagre damage, low, medium and long DNA migration, and maximum DNA damage, respectively). [d] Total comet score. [e] % *R*, reduction in comet score; NC – negative control; PC – positive control, ethyl methanesulfonate, EMS, 1 mM; $ZnA_{0.25}$ – zinc acetate dihydrate, $(Zn(CH_3COO)_2 \cdot 2H_2O)$, 0.25 mg mL^{-1}; ZnA_1 – zinc acetate dihydrate, $(Zn(CH_3COO)_2 \cdot 2H_2O)$, 1 mg mL^{-1}; ZnA_4 – zinc acetate dihydrate, $(Zn(CH_3COO)_2 \cdot 2H_2O)$, 4 mg mL^{-1}; ZnO $NP_{0.25}$ – ZnO NPs-H_2O, 0.25 mg mL^{-1}; ZnO $NP_{0.5}$ – ZnO NPs-H_2O, 0.5 mg mL^{-1}; ZnO NP_1 – ZnO NPs-H_2O, 1 mg mL^{-1}; ZnO NP_2 – ZnO NPs-H_2O, 2 mg mL^{-1}; ZnO NP_4 – ZnO NPs-H_2O, 4 mg mL^{-1}; ZnO $NP_{0.25}$ + EMS – ZnO NPs-H_2O, 0.25 mg mL^{-1} + 1 mM EMS; ZnO $NP_{0.5}$ + EMS – ZnO NPs-H_2O, 0.5 mg mL^{-1} + 1 mM EMS; ZnO NP_1 + EMS – ZnO NPs-H_2O, 1 mg mL^{-1} + 1 mM EMS; ZnO NP_2 + EMS – ZnO NPs-H_2O, 2 mg mL^{-1} + 1 mM EMS; ZnO NP_4 + EMS – ZnO NPs-H_2O, 4 mg mL^{-1} + 1 mM EMS.

The negative control showed a comet score of 27.1 ± 0.32, whereas the positive control treated with ethyl methanesulphonate (EMS) showed a markedly higher score of 111.8 ± 1.17. Comet classes 2, 3 and 4 were observed exclusively in the EMS-treated positive control, confirming the clear difference in DNA damage between the control groups under the experimental conditions.

Treatment with zinc acetate dihydrate at nominal concentrations of 0.25, 1 and 4 mg mL^{-1} resulted in comet scores of 26.9 ± 0.32, 27.4 ± 0.52 and 27.61 ± 0.71, respectively. These values were comparable to that of the negative control, and no higher comet classes (2–4) were detected in the zinc acetate-treated groups. Thus, zinc acetate did not produce a detectable increase in comet scores under the tested conditions. However, because the zinc acetate concentrations were matched to the nominal mass concentrations of the ZnO-containing material rather than to measured Zn^{2+} release, this comparison does not establish the relative contribution of soluble zinc ions to the observed DNA damage.

The effects of the tested ZnO-containing material were concentration-dependent. At 0.25 and 0.5 mg mL^{-1}, the comet scores were 27.3 ± 0.25 and 27.6 ± 0.34, respectively, and were comparable to the negative control. At 1 mg mL^{-1}, the score increased to 31.4 ± 0.68, representing a significant increase compared with the negative control, although the value remained substantially below that of the EMS-treated positive control. Further increases were observed at 2 and 4 mg mL^{-1}, with scores of 42.8 ± 0.23 and 50.04 ± 0.11, respectively. These higher concentrations differed significantly from the controls and the zinc acetate-treated groups, as reported in Table 3. Comet class 2 was observed at concentrations of 1, 2 and 4 mg mL^{-1}. Overall, the results indicate that the two lowest concentrations did not produce a detectable increase in DNA damage, whereas higher concentrations were associated with progressively increased comet scores.

The effects of co-exposure to the tested material and EMS were evaluated by comparing the comet scores of the co-treatment groups with those of the EMS-treated positive control. The calculated reductions in EMS-associated comet scores were 74.8%, 64.5% and 56.7% at 0.25, 0.5 and 1 mg mL^{-1}, respectively. At the higher concentrations of 2 and 4 mg mL^{-1}, the corresponding reductions were 38.6% and 32.8%. Thus, lower concentrations were associated with a greater reduction in the comet score relative to EMS alone, whereas the reduction was less pronounced at higher concentrations. Comet class 3 was observed in the co-treatment groups at 1, 2 and 4 mg mL^{-1}, indicating that DNA damage remained evident at these concentrations.

The co-treatment results demonstrate a concentration-dependent reduction in EMS-associated comet scores under experimental conditions. However, the percentage reduction alone does not establish a specific DNA-protective or anti-genotoxic mechanism. The observed changes may reflect a combination of effects associated with the ZnO-containing material, soluble zinc species and extract-derived constituents. Previous work has shown that an aqueous *A. eupatoria* extract alone can reduce EMS-associated comet scores.[15] Because an extract-only control was not included in the present study and

© 2026 The Author(s). Published by the Royal Society of Chemistry

the presence and amount of residual extract-derived constituents in the tested material were not determined, the contribution of these constituents cannot be separated from that of the ZnO-containing material. Furthermore, Zn^{2+} release was not quantified under the exposure conditions, preventing determination of the relative contributions of soluble zinc species. Therefore, the observed reductions cannot be attributed specifically to ZnO.

The concentration-dependent response observed in the present study is broadly consistent with previous reports showing that the genotoxic effects of ZnO-containing materials can vary with exposure concentration and experimental conditions. For example, a study of ZnO nanoparticles synthesized using *Mentha pulegium* extract reported no significant effects in the wing-spot assay at the tested doses, although increased DNA damage was observed at the highest concentrations in the comet assay.[46] Another study reported detectable DNA strand breaks in *D. melanogaster* haemocytes only at higher ZnO nanoparticle doses.[21] In addition, previous work has reported no significant increase in DNA damage or mutant clone formation under certain exposure conditions, despite evidence of nanoparticle uptake and changes in gene expression.[47] These differences highlight the importance of nanoparticle characteristics, dose and experimental design when interpreting genotoxicity results.

Several limitations should be considered when interpreting the present findings. First, the absence of an extract-only control prevents the effects of extract-derived compounds from being separated from those of the ZnO-containing material. Second, Zn^{2+} release was not measured under the actual exposure conditions; therefore, the contribution of soluble zinc to the observed DNA damage cannot be established. Third, larval survival and general toxicity were not independently quantified during the 24 h exposure period. Consequently, the potential influence of general toxicity on the observed comet scores cannot be excluded. Lower comet scores in the co-treatment groups cannot be attributed solely to a DNA-protective effect, as they may also reflect differences in effective EMS exposure, interactions between EMS and constituents of the tested material, or the loss of highly damaged cells. These possibilities were not directly investigated in the present study and should therefore be considered alternative explanations rather than demonstrated mechanisms. Finally, comet scoring was not performed under blind conditions. Although the results are based on three independent experiments, the absence of blind scoring represents a methodological limitation that should be considered when interpreting the findings.

Taken together, the alkaline comet assay showed that the tested ZnO-containing material was associated with concentration-dependent changes in DNA damage in *D. melanogaster*. The two lowest concentrations (0.25 and 0.5 mg mL^{-1}) did not produce a detectable increase in comet scores compared with the negative control, whereas higher concentrations were associated with increased DNA damage. Co-exposure with EMS resulted in lower comet scores than EMS treatment alone, particularly at the lower concentrations. However, in the absence of toxicity measurements, an extract-only control and blinded comet scoring, these findings should be interpreted cautiously as reductions in EMS-associated comet scores under the tested conditions, rather than as definitive evidence of a DNA-protective or antigenotoxic effect attributable specifically to ZnO.

The study involved experiments using *Drosophila melanogaster*. All experimental procedures were conducted in accordance with applicable institutional guidelines and established standards for the care and use of *Drosophila melanogaster* in research. Ethical approval was not required for experiments involving *Drosophila melanogaster* under the applicable institutional regulations.

4 Conclusion

In the present study, a ZnO-containing material was prepared in the presence of an aqueous extract of *A. eupatoria* and characterized using complementary spectroscopic and electron-microscopy techniques. TEM and selected-area electron diffraction (SAED) provided evidence of crystalline ZnO in the examined regions, while XPS revealed zinc predominantly in the +2-oxidation state and surface-associated oxygen- and carbon-containing species. TEM analysis showed predominantly elongated and irregularly shaped particles, with measured dimensions ranging from approximately 40 to 220 nm. However, the absence of bulk X-ray diffraction (XRD) analysis means that the phase composition and purity of the entire powder could not be conclusively established.

The biological assays revealed concentration- and microorganism-dependent antimicrobial activity, with MIC values varying substantially across the bacterial and fungal strains tested. The preparation also produced cell-type- and exposure-time-dependent changes in MTT assay signals in cancer and non-malignant cell models. Although the apparent MTT-based IC_{50} values indicated differences in cellular responses, the absence of cell-free interference controls and an independent viability assay limits the interpretation of these results and does not establish selective anticancer activity.

Changes in NBT and Griess assay signals and in total NF-κB p65 levels were observed under the tested conditions. These findings indicate changes in redox-associated and inflammatory-associated assay responses, but do not establish direct intracellular reactive oxygen species generation, activation or inhibition of the NF-κB signaling pathway, or a confirmed anti-inflammatory mechanism.

In the *Drosophila melanogaster* alkaline comet assay, the two lowest concentrations tested (0.25 and 0.5 mg mL^{-1}) did not produce a detectable increase in DNA damage compared with the negative control, whereas higher concentrations were associated with increased comet scores. Co-exposure with EMS resulted in lower comet scores than EMS treatment alone, particularly at the lower concentrations. This finding should be interpreted as a reduction in EMS-associated comet scores under experimental conditions rather than definitive evidence of a DNA-protective or antigenotoxic mechanism.

Several limitations affect the interpretation of the overall findings. Plant-free ZnO and extract-only controls were not

© 2026 The Author(s). Published by the Royal Society of Chemistry

included, Zn^{2+} release was not quantified under the relevant biological exposure conditions, and potential interference with the colorimetric and redox-based assays could not be excluded. In addition, bulk purity, colloidal stability in biological media, and larval survival and general toxicity during the comet assay exposure were not independently established. Consequently, the individual contributions of the ZnO-containing material, soluble zinc species and extract-derived constituents remain unresolved.

Overall, the study demonstrates that the tested ZnO-containing preparation exhibits measurable physicochemical characteristics and a range of biological responses under the experimental conditions investigated. Further work incorporating appropriate component-specific controls, bulk structural characterization, exposure-relevant Zn^{2+} measurements, assay-interference controls and independent validation of biological endpoints is required to establish the reproducibility, mechanisms and potential applications of this material.

Author contributions

Katarina Marković: conceptualization, methodology, investigation, writing – original draft. Ana Kesić: investigation, methodology, nanoparticle synthesis. Đorđe Minić: methodology, nanoparticle synthesis. Nevena Djukić: investigation, validation, data curation, nanoparticle synthesis. Nadežda Radmilović: methodology, transmission electron microscopy (TEM) characterization. Maja Popović: formal analysis, X-ray photoelectron spectroscopy (XPS) analysis and interpretation. Sanja Matić: methodology, DNA-damage and DNA-damage-modulation studies. Milica Paunović: methodology, cytotoxicity and inflammatory-response studies. Ana D. Obradović: methodology, cytotoxicity and inflammatory-response studies. Mirjana Grujović: methodology, formal analysis, antimicrobial studies, writing – review & editing. All authors reviewed and approved the final version of the manuscript.

Conflicts of interest

The authors declare that they have no known competing financial interests or personal relationships that could have appeared to influence the work reported in this paper. The authors alone are responsible for the content and writing of this manuscript.

Abbreviations

ZnO NPs	Zinc oxide nanoparticles
NPs	Nanoparticles
$Zn(CH_3COO)_2$	Zinc acetate
TEM	Transmission electron microscopy
UV-vis	Ultraviolet-visible spectroscopy
FTIR	Fourier-transform infrared spectroscopy
DMEM	Dulbecco's modified eagle medium
EB	Ethidium bromide
MTT	3-[4,5-Dimethylthiazol-2-yl]-2,5-diphenyltetrazolium bromide
PBS	Phosphate-buffered saline
NMA	Normal melting point agarose
LMA	Low melting point agarose
EMS	Ethyl methane sulphonate
HRTEM	High-resolution transmission electron microscopy
STEM	Scanning transmission electron microscopy
HAADF	High-angle annular dark-field imaging
EDS	Energy-dispersive X-ray spectroscopy
DMSO	Dimethyl sulfoxide

Data availability

The data supporting the findings of this study are available from the corresponding author upon reasonable request.

Acknowledgements

This research was funded by the Ministry of Education and the Ministry of Science, Technological Development and Innovation of the Republic of Serbia (Grant No. 451-03-33/2026-03/200378 and 451-03-34/2026-03/200122). ChatGPT (OpenAI) was used for language editing, grammatical corrections, and improving manuscript readability, as well as for assisting with the visual layout, organisation, and resolution optimisation of the graphical abstract. All scientific images and experimental results presented in the graphical abstract originate from the authors' original research. AI was not used for data generation, data analysis, or scientific interpretation. The authors reviewed and verified all content and take full responsibility for the final manuscript.

References

1 S. Kulshrestha and A. U. Khan, *IET Nanobiotechnol.*, 2018, **12**, 1009–1017, DOI: 10.1049/iet-nbt.2018.5112.
2 A. Desai, S. Ghosh, S. Sankaranarayanan, D. Bhatia and A. K. Yadav, *Mater. Adv.*, 2025, **6**, 6612–6647, DOI: 10.1039/D5MA00487J.
3 X.-Q. Zhou, Z. Hayat, D.-D. Zhang, M.-Y. Li, S. Hu, Q. Wu, Y.-F. Cao and Y. Yuan, *Processes*, 2023, **11**, 1193, DOI: 10.3390/pr11041193.
4 V. R. Lebaka, P. Ravi, M. C. Reddy, C. Thummala and T. K. Mandal, *Nanomaterials*, 2025, **15**, 754, DOI: 10.3390/nano15100754.
5 A. M. Mohammed, M. Mohammed, J. K. Oleiwi, F. H. Ihmedee, T. Adam, B. O. Betar and S. C. B. Gopinath, *Nano TransMed*, 2025, **4**, 100097, DOI: 10.1016/j.ntm.2025.100097.
6 D. Alqaffaf, A. M. Atoom, R. Abu Huwaij, M. A. H. A. Abusalah, B. T. Alzubi, A. Al-Kaabneh, M. A. H. A. Abusalah and M. A. Sughayer, *PLoS One*, 2026, **21**, e0340470, DOI: 10.1371/journal.pone.0340470.
7 S. Anjum, M. Hashim, S. A. Malik, M. Khan, J. M. Lorenzo, B. H. Abbasi and C. Hano, *Cancers*, 2021, **13**, 4570, DOI: 10.3390/cancers13184570.

© 2026 The Author(s). Published by the Royal Society of Chemistry

8 G. Gahlawat and A. R. Choudhury, *RSC Adv.*, 2019, **9**, 12944–12967, DOI: 10.1039/C8RA10483B.

9 M. Soni, P. Mehta, A. Soni and G. K. Goswami, *IOSR J. Biotechnol. Biochem.*, 2018, **4**, 78–83, DOI: 10.9790/264X-0403017883.

10 G. Pal, P. Rai and A. Pandey, in *Green Synthesis, Characterization and Applications of Nanoparticles*, ed. A. K. Shukla and S. Iravani, Elsevier, Amsterdam, 2019, pp. 1–26.

11 A. Roychoudhury, *Indian J. Pharm. Biol. Res.*, 2020, **8**, 26–31, DOI: 10.30750/ijpbr.8.3.4.

12 M. M. Khan, S. N. Matussin and A. Rahman, *Bioprocess Biosyst. Eng.*, 2022, **45**, 619–645, DOI: 10.3390/ph17121711.

13 I. A. Baba, O. B. Awe, S. Mustapha, M. A. Abubakar, A. S. Abdulkareem, J. O. Tijani and K. S. Obayomi, *Hybrid Adv.*, 2026, **13**, 100666, DOI: 10.1016/j.hybadv.2026.100666.

14 M. Ž. Muruzović, K. G. Mladenović, O. D. Stefanović, S. M. Vasić and L. R. Čomić, *J. Food Drug Anal.*, 2016, **24**, 539–547, DOI: 10.1016/j.jfda.2016.02.007.

15 K. Marković, A. Kesić, M. Novaković, M. Grujović, D. Simijonović, E. Avdović, S. Matić, M. Paunović, M. Milutinović, D. Nikodijević, O. Stefanović and Z. Marković, *RSC Adv.*, 2024, **14**, 4591–4606, DOI: 10.1039/D3RA07819A.

16 W. S. Rasband, *ImageJ*, U.S. National Institutes of Health, Bethesda, MD, USA, 1997–2018, https://imagej.net/ij/.

17 S. D. Sarker, L. Nahar and Y. Kumarasamy, *Methods*, 2007, **42**, 321–324, DOI: 10.1016/j.ymeth.2007.01.006.

18 T. Mosmann, *J. Immunol. Methods*, 1983, **65**, 55–63, DOI: 10.1016/0022-1759(83)90303-4.

19 C. Auclair and E. Voisin, in *Handbook of Methods for Oxygen Radical Research*, ed. R. A. Greenwald, CRC Press, Boca Raton, 1985, pp. 123–132.

20 L. C. Green, D. A. Wagner, J. Glogowski, P. L. Skipper, J. S. Wishnok and S. R. Tannenbaum, *Anal. Biochem.*, 1982, **126**, 131–138, DOI: 10.1016/0003-2697(82)90118-X.

21 E. R. Carmona, T. N. Guecheva, A. Creus and R. Marcos, *Environ. Mol. Mutagen.*, 2011, **52**, 165–169, DOI: 10.1002/em.20604.

22 I. Mukhopadhyay, D. K. Chowdhuri, M. Bajpayee and A. Dhawan, *Mutagenesis*, 2004, **19**, 85–90, DOI: 10.1093/mutage/geh007.

23 H. R. Siddique, D. K. Chowdhuri, D. K. Saxena and A. Dhawan, *Mutagenesis*, 2005, **20**, 285–290, DOI: 10.1093/mutage/gei032.

24 N. P. Singh, M. T. McCoy, R. R. Tice and E. L. Schneider, *Exp. Cell Res.*, 1988, **175**, 184–191, DOI: 10.1016/0014-4827(88)90265-0.

25 Ü. Özgür, Y. I. Alivov, C. Liu, A. Teke, M. A. Reshchikov, S. Doğan, V. Avrutin, S.-J. Cho and H. Morkoç, *J. Appl. Phys.*, 2005, **98**, 041301, DOI: 10.1063/1.1992666.

26 G. Sangeetha, S. Rajeshwari and R. Venckatesh, *Mater. Res. Bull.*, 2011, **46**, 2560–2566, DOI: 10.1016/j.materresbull.2011.07.046.

27 M. Bin Ali, T. Iftikhar and H. Majeed, *Heliyon*, 2024, **10**, e37927, DOI: 10.1016/j.heliyon.2024.e37927.

28 J. Pasquet, Y. Chevalier, J. Pelletier, E. Couval, D. Bouvier and M.-A. Bolzinger, *Colloids Surf., A*, 2014, **457**, 263–274, DOI: 10.1016/j.colsurfa.2014.05.057.

29 M. J. Hajipour, K. M. Fromm, A. A. Ashkarran, D. Jimenez de Aberasturi, I. R. de Larramendi, T. Rojo, V. Serpooshan, W. J. Parak and M. Mahmoudi, *Trends Biotechnol.*, 2012, **30**, 499–511, DOI: 10.1016/j.tibtech.2012.06.004.

30 S. Adhikari, R. Gupta, A. Surin, T. S. Kumar, S. Chakraborty, D. Sarkar and G. Madras, *RSC Adv.*, 2016, **6**, 80086–80098, DOI: 10.1039/c6ra10472j.

31 S. Sharma, K. Kumar, N. Thakur, S. Chauhan and M. S. Chauhan, *Bull. Mater. Sci.*, 2020, **43**, 20, DOI: 10.1007/s12034-019-1986-y.

32 B. L. da Silva, M. P. Abuçafy, E. Berbel Manaia, J. A. Oshiro Junior, B. G. Chiari-Andréo, R. C. R. Pietro and L. A. Chiavacci, *Int. J. Nanomed.*, 2019, **14**, 9395–9410, DOI: 10.2147/IJN.S216204.

33 S. E. Jin, J. E. Jin, W. Hwang and S. W. Hong, *Int. J. Nanomed.*, 2019, **14**, 1737–1751, DOI: 10.2147/IJN.S192277.

34 L. Kaliraj, J. C. Ahn, E. J. Rupa, S. Abid, J. Lu and D. C. Yang, *J. Photochem. Photobiol., B*, 2019, **199**, 111588, DOI: 10.1016/j.jphotobiol.2019.111588.

35 S.-E. Jin and H.-E. Jin, *Nanomaterials*, 2021, **11**, 263, DOI: 10.3390/nano11020263.

36 J. Jeevanandam, S. F. Kiew, S. Boakye-Ansah, S. Y. Lau, A. Barhoum, M. K. Danquah and J. Rodrigues, *Nanoscale*, 2022, **14**, 2534–2571, DOI: 10.1039/D1NR08141D.

37 M. C. Sportelli, C. Gaudiuso, A. Volpe, M. Izzi, R. A. Picca, A. Ancona and N. Cioffi, *Reactions*, 2022, **3**, 423–441, DOI: 10.3390/reactions3030031.

38 R. Rohani, N. S. F. Dzulkharnien, N. H. Harun and I. A. Ilias, *Bioinorg. Chem. Appl.*, 2022, **2022**, 3077747, DOI: 10.1155/2022/3077747.

39 S. Redjili, H. Ghodbane, H. Tahraoui, L. Abdelouahed, D. Chebli, M. S. Ola, A. A. Assadi, M. Kebir, J. Zhang, A. Amrane and S. Lekmine, *Catalysts*, 2025, **15**, 256, DOI: 10.3390/catal15030256.

40 R. Hamed, R. Z. Obeid and R. Abu-Huwaij, *Nanotechnol. Rev.*, 2023, **12**, 20230112, DOI: 10.1515/ntrev-2023-0112.

41 N. Rodríguez-Barajas, M. D. Ponce-Regalado, M. S. Segura-Almendárez, C. M. Rodríguez-Razon, S. Ghotekar, M. Fellah and A. Pérez-Larios, *Results Chem.*, 2024, **9**, 101654, DOI: 10.1016/j.rechem.2024.101654.

42 M. Conte, V. Vighetto and V. Cauda, *Expert Opin. Drug Delivery*, 2026, **23**, 975–987, DOI: 10.1080/17425247.2026.2638409.

43 H. Maheswaran, S. Djearamane, A. C. T. A. Dhanapal and L. S. Wong, *Heliyon*, 2024, **10**, e31316, DOI: 10.1016/j.heliyon.2024.e32367.

44 K. Lingappan, *Curr. Opin. Toxicol.*, 2018, **7**, 81–86, DOI: 10.1016/j.cotox.2017.11.002.

45 S. Liu, J. Liu, Y. Wang, F. Deng and Z. Deng, *MedComm*, 2025, **6**, e70268, DOI: 10.1002/mco2.70268.

46 D. Akyil and E. Yeniyol, *Toxicol. Res.*, 2025, **14**, tfaf046, DOI: 10.1093/toxres/tfaf046.

47 M. Alaraby, B. Annangi, A. Hernández, A. Creus and R. Marcos, *J. Hazard. Mater.*, 2015, **296**, 166–174, DOI: 10.1016/j.jhazmat.2015.04.053.

© 2026 The Author(s). Published by the Royal Society of Chemistry